Development of PSMA-1007 - Related Series of 18F-Labeled Glu-ureido type PSMA inhibitors.

Journal of Medicinal Chemistry 63(2020)19, 10897-10907

DOI: https://doi.org/10.1021/acs.jmedchem.9b01479

Development of PSMA-1007 - Related Series of ^{18}F-Labeled Glu-ureido type PSMA inhibitors

Jens Cardinale[*,†,#], Mareike Roscher[†], Martin Schäfer[†], Max Geerlings[†], Martina Benešová[†], Ulrike Bauder-Wüst[†], Yvonne Remde[†], Matthias Eder[†,⊥], Zora Nováková[‡], Lucia Motlová[‡], Cyril Barinka[‡], Frederik L. Giesel[§], Klaus Kopka[†,I]

†Division of Radiopharmaceutical Chemistry, German Cancer Research Center, INF 280, 69239 Heidelberg, Germany.

‡Laboratory of Structural Biology, Institute of Biotechnology of the Czech Academy of Sciences, BIOCEV, Prumyslova 595, 252 50 Vestec, Czech Republic.

§Department of Nuclear Medicine, University Hospital Heidelberg, INF 400, 69239 Heidelberg, Germany.

Abstract: In recent years, a number of drugs targeting the prostate specific-membrane antigen (PSMA) have become important tools in the diagnosis and treatment of prostate cancer. In the present work, we report on the synthesis and preclinical evaluation of a series of ^{18}F-labeled PSMA ligands for diagnostic application based on the theragnostic ligand PSMA-617. By applying modifications to the linker-structure, insight into the structure-activity relationship could be gained highlighting the importance of hydrophilicity and stereoselectivity on interaction with PSMA and hence the biodistribution. Selected compounds were co-crystallized with the PSMA-protein and analyzed by X-ray with mixed results. Amongst these, PSMA-1007 (compound 5) showed the best interaction with the PSMA protein. The respective radiotracer [^{18}F]PSMA-1007 was translated into the clinic and is in the meantime subject of advanced clinical trials.

Introduction

Over the past years, radiolabeled ligands targeting the prostate-specific membrane antigen (PSMA, also known as glutamate carboxypeptidase II or GCP-II) have become the new gold standard for the diagnosis of prostate cancer in nuclear medicine outperforming radiolabeled choline derivatives as well as [^{18}F]FACBC in particular for recurrent disease with low PSA levels.[1-12] Currently, ^{68}Ga-labeled PSMA-ligands are used most frequently for positron emission tomography (PET) in clinical application.[13-18] However, commercially available ^{68}Ge/^{68}Ga generators only offer a maximum activity of up to 1.85 GBq ^{68}Ga per elution limiting the average batch production of a respective tracer to 2 to 4 patient doses. Thus, sustaining clinical routine demands multiple tracer syntheses per day – a problem that might be overcome by ^{18}F-labeled PSMA-ligands. Another decisive advantage of ^{18}F-labeled tracers is the possibility of shipment to distant facilities - the so called satellite concept.

In order to develop novel radiofluorinated PSMA-ligands for the diagnosis of prostate cancer, PSMA-617 was chosen as lead structure (structure depicted in Scheme 2).[19,20] This tracer offers wide opportunities for radiolabeling with different radionuclides for imaging and therapy via its chelator DOTA and its use is of great potential in clinical settings.[21,22] The main development steps are summarized in scheme 1. The chelator was replaced by fluoronicotinic acid to allow for easy introduction of fluorine-18 into the molecule (see below). From the development of PSMA-617 it was already known, that the hydrophobic aminoacids in the linker play a critical role for the affinity and uptake of PSMA ligands.[20] Thus, only minor modifications in this area were considered.[23] However, it quickly turned out that the replacement of DOTA by 6-fluoronicotinic acid and the resulting loss of hydrophilicity negatively impacted the bio distribution.[23,24] Thus, additional hydrophilic amino acids were added to the linker eventually leading to the development of [^{18}F]PSMA-1007,[24] which was successfully translated into clinic and is now subject of advanced clinical trials.[25-32] While initial preclinical characterization of [^{18}F]PSMA-1007 was already published,[25] we herein report on its development.

Scheme 1. Key steps in the development of PSMA-1007 and linker structure [23,24]

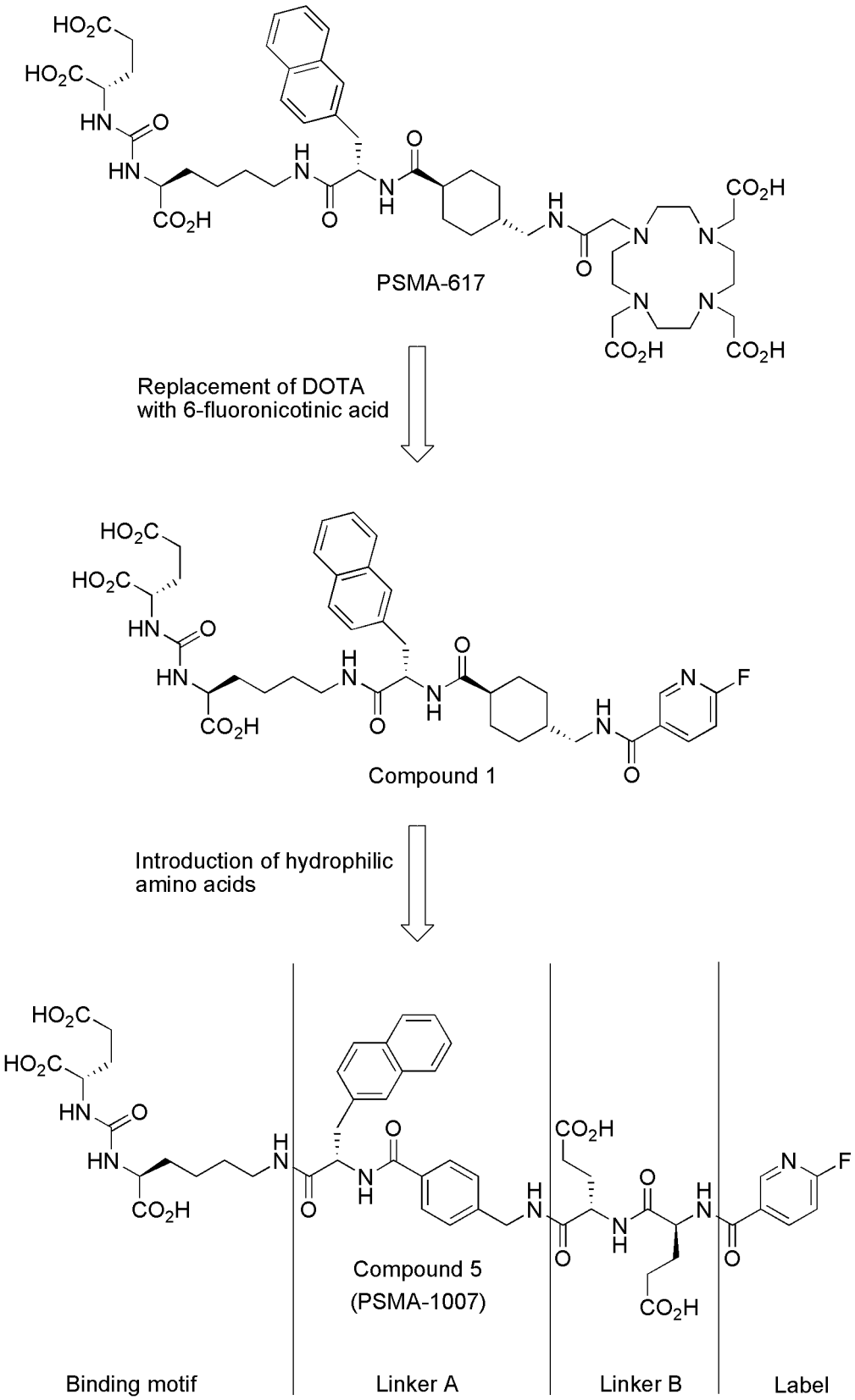
PSMA-617
Replacement of DOTA
with 6-fluoronicotinic acid
Compound 1
Introduction of hydrophilic
amino acids
Compound 5
(PSMA-1007)
Binding motif
Linker A
Linker B
Label

Introduction of fluorine-18 was accomplished using a two-step procedure via the intermediate 6-[^{18}F]fluoronicotinic acid 2,3,5,6-tetrafluorophenyl ester ([^{18}F]F-Py-TFP, Scheme 2) for its quickness and simplicity.[33]

Scheme 2: Labeling Procedure using [^{18}F]F-Py-TFP[a]

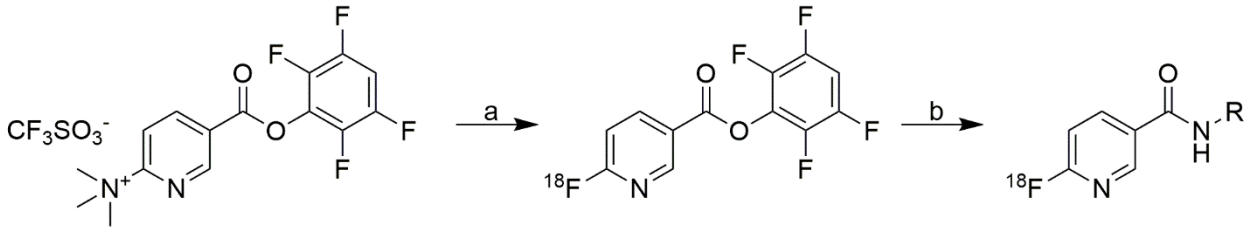

[a]Reagents and conditions (see also ref. 12): (a) 10 mg precursor, (Bu_4N^+)(HCO_3^-/F^-), *t*-BuOH/MeCN (8:2), 40 °C, 5-10 min; (b) 2-4 mg R-NH_2, buffer pH 8.5-9.0.

Results

General structure of the ligands. The general structure of the investigated ligands is indicated in scheme 1 exemplified by PSMA-1007 (compound **5** in the following text). For clarity, the ligands prepared during the present study were divided into four sets. In sets I and IV modifications of lipophilic linker A are investigated, while sets II and III focus on modifications of the hydrophilic linker B. The linker structures of all compounds discussed in this paper are summarized in Figure 1.

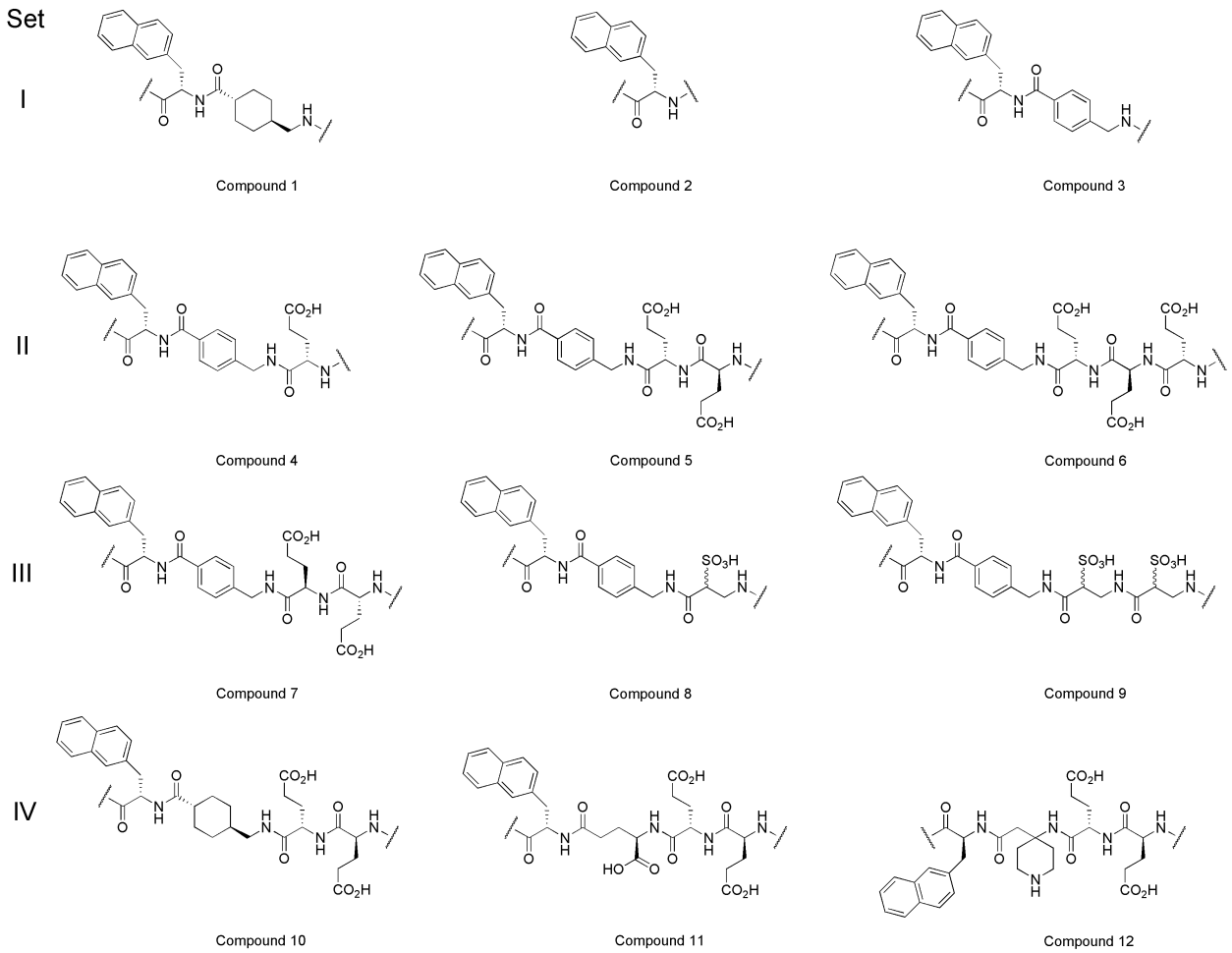

Figure 1. Linker structures (A and B) of the compounds of the present study. Binding motif and label have been omitted for clarity.

***In vitro* and *in vivo* evaluation of the ligands.** All ligands were evaluated regarding binding affinity, specific cell binding, and internalization using PSMA-positive LNCaP cells. The results are summarized in Table 1. Compounds **3** and **5** (see discussion) were further investigated in organ distribution and dynamic PET experiments. The main results are summarized in Table 2 and Figure 2, respectively. The corresponding time-activity curves are given in the supporting information (Figures S1 and S2).

Table 1. Summary of binding characteristics of all ligands evaluated in this study

Compound	Set	K_i[a] [nM]	Internalization[b] [%IA/10^5 cells]	Surface bound[b] [%IA/10^5 cells]	Internalized fraction[c] [%]
1	I	2.2±1.2*	1.9±0.9	0.54±0.22	23.1±2.7
2	I	3.6±0.5*	1.8±1.3	1.3±1.4	33.2±16.7
3	I	2.9±0.5*	1.7±0.6	1.4±9.7	44.3±6.1
4	II	10.4±3.0	1.9±1.1	0.75±0.54	27.2±2.6
5	II	6.7±1.7	0.24±0.07	0.58±0.31	68.9±4.8
6	II	11.4±3.3	0.09±0.07	0.07±0.03	49.8±17.0
7	III	6.9±1.1	0.93±0.07	0.21±0.10	19.9±11.8
8	III	12.2±2.7	0.17±0.04	0.17±0.05	50.5±4.1
9	III	6.0±0.3	0.10±0.04	0.24±0.16	67.2±7.1
10	IV	10.3±2.3	0.77±0.31	0.21±0.02	22.3±5.2
11	IV	7.4±2.8	0.65±0.20	0.16±0.04	20.7±2.8
12	IV	108*	-	-	-

[a]Competitive binding assay. Each independent experiment represents a quadruplicate. [b]Cellular uptake. Each independent experiment represents a triplicate. [c]Equals internalization / (internalization + surface bound). If not stated otherwise all values are an average from two or three independent experiments. The asterisk (*) indicates single experiments. Cellular uptake of compound **5** was determined with n = 9 and was in part previously reported.[13]

Table 2. Results of the organ distribution experiments

Organ	Uptake [%ID/g]	
	[^{18}F]3	**[^{18}F]5**
Blood	2.02±2.65	0.60±0.21
Heart	0.25±0.01	1.11±0.20
Lung	0.65±0.04	1.25±0.27
Spleen	1.96±0.08	6.99±1.04
Liver	3.02±1.31	1.06±0.20

Kidney	32.37±2.91	84.03±13.85
Muscle	0.25±0.04	0.79±0.28
Small intestine	8.49±5.17	0.90±0.21
Brain	0.07±0.01	0.12±0.04
Tumor	3.40±0.59	8.04±2.39
Tumor-to-muscle	13.6±3.2	10.2±4.7
Tumor-to-blood	1.7±2.2	13.2±6.1

All mice (n = 3) were injected with 1-2 MBq **[^{18}F]3** or **[^{18}F]5** (60 pmol in 100 µl; n = 3) *via* tail vein. The mice were bearing PSMA-positive LNCaP tumors. Values for compound **5** were previously reported.[13]

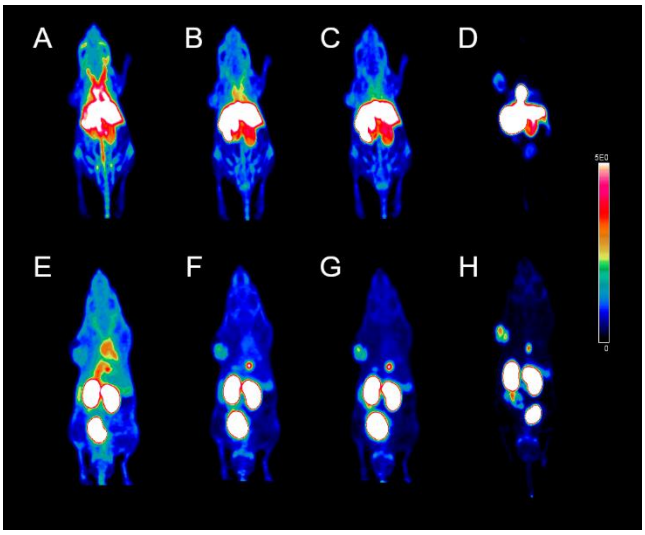

Figure 2. Maximum intensity projections of LNCaP tumor-bearing mice injected with approx. 25 MBq (60 pmol in 100 µl) **[^{18}F]3** (A-D) or **[^{18}F]5** (E-F). Images were acquired 0-20 min (A,E), 20-40 min (B,F), 40-60 min (C,G) and 100-120 min (D,H) p.i.. Images E-H were published previously.[13]

Crystal structures of selected PSMA/inhibitor complexes. Crystal structures of PSMA/inhibitor complexes were determined to the resolution limit of 1.43 Å, 1.65 Å, and 1.53 Å

for compounds **5**, **7**, and **9**, respectively. The interpretable positive electron density representing the active site-bound ligand was observed for all complexes, and individual compounds were fitted into the positive peaks of the *Fo-Fc* electron density map in the final stages of the refinement (Figure 3).

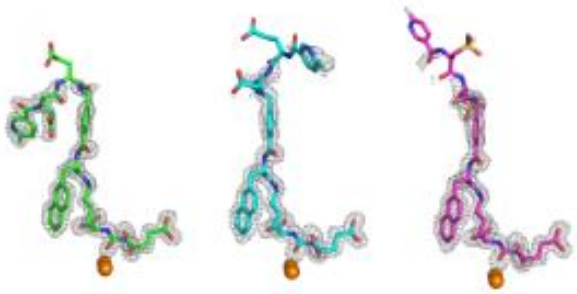

Figure 3. The Fo-Fc omit map (grey) is contoured at 3.0 σ and inhibitors are shown in stick representation with atoms colored red (oxygen), blue (nitrogen), pale cyan (fluorine), and yellow (sulfur). Carbon atoms are colored green, cyan and purple for compound **5** (PDB:ID 5O5T), compound **7** (PDB:ID 5O5R), and compound **9** (PDB:ID 5O5U), respectively. The active-site zinc ions are shown as orange spheres. Notice the absent electron density for some distal inhibitor parts implying its positional flexibility due to missing interactions with the enzyme.

Positioning of the P1' glutamate/urea docking module into the S1' pocket, together with all inhibitor/protein interactions, is virtually identical to canonical urea-based inhibitors, complexes of which were described previously. Similarly, the P1 carboxylate function forms hydrogen bonding interactions with side chains of Asn519, Arg534, and Arg536 replicating thus the known interaction pattern of analogous PSMA/urea complexes.[34-37]

The introduction of the 1-L-alanylnapht-2-yl function into the linker region represents a novel motif with unknown interaction interface with PSMA. Interestingly, our structures reveal that the

1-L-alanylnapht-2-yl function folds back onto the aminohexanoyl moiety and occupies a shallow pocket on the wall of the entrance funnel delineated by the side chains of Glu457, Tyr549, Tyr552, Tyr700, and the main chain of Gly548. It concomitantly pushes the aminohexanoyl group to the opposite side of the funnel and when combined, these two functions fill effectively (and completely) the lower portion of the funnel. The adjacent benzoyl group, forms the direct H-bond with the side chain amide of Asn698 (2.9 Å) and additional water-mediated contacts with the main-chain carbonyl of Lys207 (3.1 Å) and Phe536 (2.6 Å). Furthermore, the phenyl ring is packed against the methyl group of Ala701 (3.5 Å from the ring center) contributing thus weak methyl/π attraction force between PSMA and the inhibitor.

Contrary to the invariant placement of the binding motif and the linker A, the distal inhibitor parts, i.e. the hydrophilic linker B together with the label moiety, occupy diverse positions in the three complexes. Compound **5** is the only inhibitor in this series, where the distal parts are fully defined in the *Fo-Fc* omit map (Figure 3). While the LGlu-LGlu linker does not form any direct contacts with PSMA, the fluoro-pyridine label is inserted into the arene-binding site (ABS) (Figure 4), a shallow pocket at the PSMA surface defined by side chains of Trp541, Arg511 and Arg463.[16] The *Fo-Fc* electron density maps for distal parts of **7** and **9** are less clear or missing, and this fact is consistent with the absence of pronounced intermolecular interactions with PSMA and resulting positional flexibility of this function outside the internal funnel of PSMA. In the case of **7**, which differs from **5** only by the stereochemistry of linker glutamates, the DGlu-DGlu linker is not visible in the structure, while the weak *Fo-Fc* electron density peaks of the terminal label group are observed close to the interface of helices α4 (amino acids Thr182 – Arg190) and α19 (amino acids Pro706 – Leu712). For **9**, only the proximal sulfo-alanyl moiety, engaged in H-bonding/ionic

interactions with Ser513 (3.4 Å) and Lys514 (2.9 and 3.4 Å), is visible in the structure, while the remaining inhibitor parts are completely disordered.

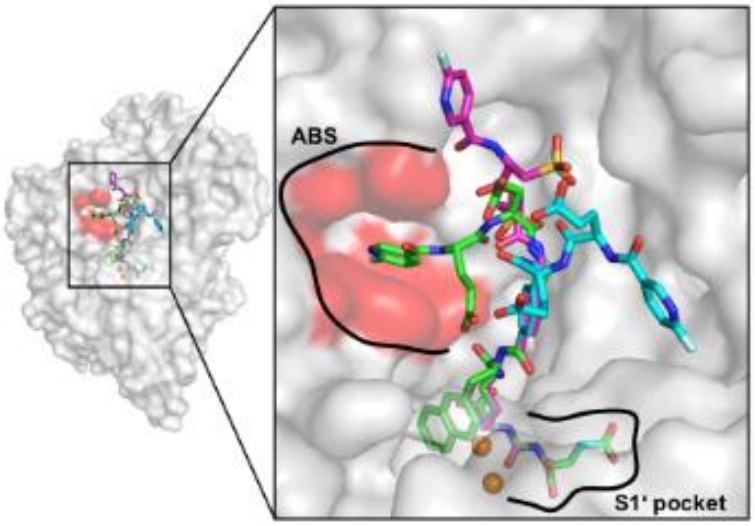

Figure 4. The superposition of PSMA/inhibitor complexes (from PDB-IDs 5O5T, 5O5R and 5O5U). PSMA molecules in individual complexes were superpositioned on corresponding C-α atoms. PSMA is shown in semitransparent surface representation and individual inhibitors in stick representation with carbon atoms colored green, cyan and purple for **5**, **7**, and **9**, respectively. The arene binding site (ABS) is marked red. Notice different positioning of the distal part of the inhibitors, while the PSMA binding motifs up to the phenyl ring fully overlap.

Discussion

Compound set I (preliminary ligand set). In the first compound set, the simplest derivatives of PSMA-617 using the 6-fluoronicotinic acid prosthetic group were investigated (compound **1**-**3**). The aim within this set was the validation of our structural approach. All three compounds exhibited a high binding affinity towards PSMA in the low nanomolar range and showed good

internalization ratios on LNCaP cells, ranging from 23 to 44 %. With the highest internalized fraction of 44 % and a good affinity of 2.9 nM compound **3** was selected for further *in vivo* experiments.

In the organ distribution, compound **3** showed a moderate tumor uptake of 3 % ID/g with a tumor-to-blood ratio of 1.68 and a tumor-to-muscle ratio of 12.2. However, a considerable uptake in spleen, kidneys, liver and small intestine was also observed. While the uptake in kidneys is endogenous and specific for PSMA binding ligands, the undesired uptake in liver and small intestine indicate a hepatobiliary excretion of the tracer. This might be a consequence of the loss in hydrophilicity caused by replacement of the chelator moiety with the prosthetic group. Finally, compound **3** was also investigated in a dynamic PET scan in an LNCaP tumor-bearing mouse. Compared to the organ distribution experiment, the observed tumor-to-blood and tumor-to-muscle ratios, calculated from the respective standardized uptake values (SUV; blood corresponds to heart), were lower with values of 0.71 and 3.0, respectively. This is also reflected in the maximum intensity projections (MIPs), where the tumor is only barely visualized at 60 min p.i.. At 120 min p.i., the visualization is clearly improved. From these very first results we concluded, that further ligands should exhibit an enhanced hydrophilicity.

Compound set II. In this set, we aimed towards ligands with an enhanced hydrophilicity by the systematic addition of glutamic acids to the linker structure counterbalancing the loss of hydrophilicity compared to PSMA-617 by the elimination of the DOTA chelator. Therefore, the compounds are also compared with compound **3** (with the number of Glu units = 0). All compounds show a high affinity towards PSMA in competitive cell binding studies while the internalized fraction varies in a non-systematic manner. To compensate for inter-assay variability, all compounds were compared on a single 24 well plate using LNCaP cells from the same passage

(Figure 5). While the total specific binding of compound **3** is significantly higher than that of the other compounds, compound **5** clearly shows the highest internalization ratio, which was considered as crucial value for mimicking the *in vivo* behavior of PSMA-617 based therapeutics.

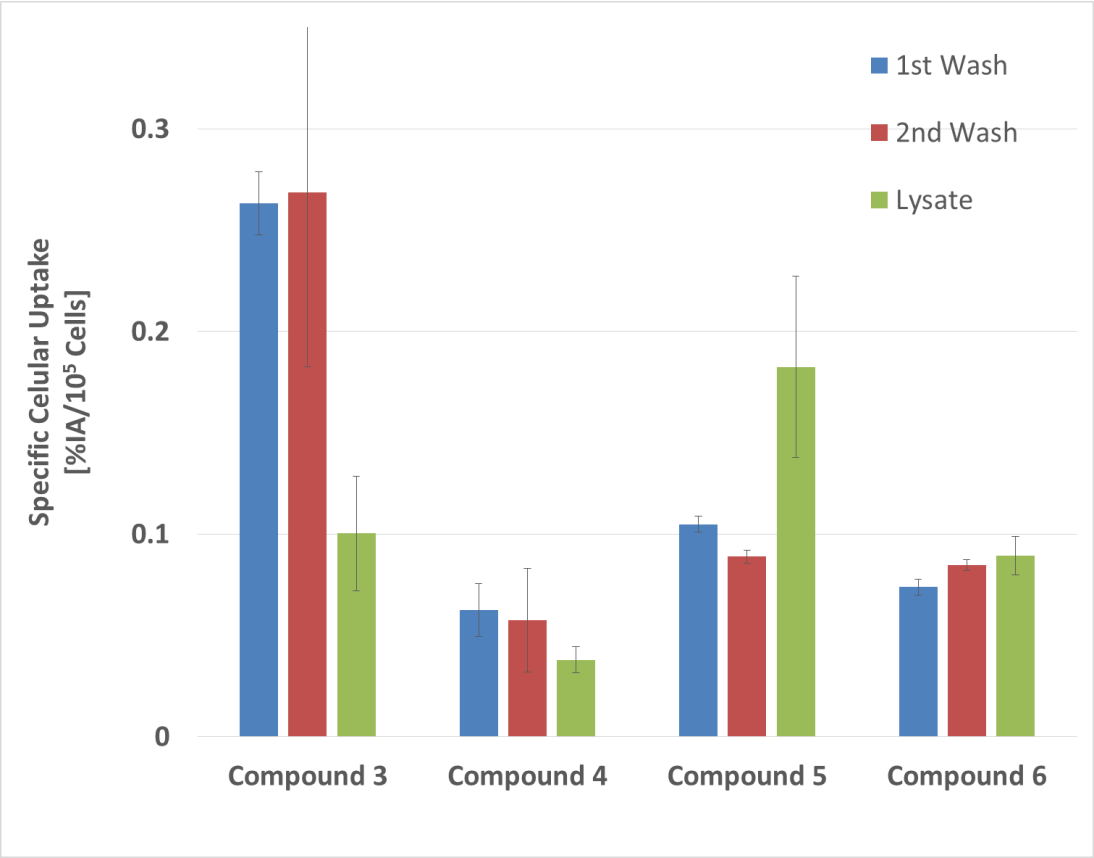

Figure 5. Example of a cell binding assay (n = 1); All compounds were measures as triplet. 1st and second wash corresponds to surface bound activity, lysate to internalized activity.

Therefore, compound **5** was further evaluated in LNCaP tumor-bearing nude mice. The organ distribution revealed a significantly increased uptake in the kidneys, while the uptake decreased in liver and small intestine. This clearly indicates the desired shift from hepatobiliary towards renal excretion. Furthermore, compound **5** demonstrated an improved tumor-to-blood ratio in comparison to compound **3**, while the tumor-to-muscle ratio slightly decreased. In the following dynamic PET experiment **[^{18}F]5** clearly outperformed compound **3** (Figure 2) reflecting the

increased tumor uptake. Therefore, we selected compound **5** as new lead structure for further development.

Compound Set III. In this set, we tried to replace the glutamic acids in linker B by non-canonical, negatively charged amino acids. All compounds showed acceptable binding affinities to PSMA. Interestingly, replacing the natural L-glutamic acids in linker B of compound **5** by non-natural D-glutamic acids in compound **7** resulted in a significant reduction of the internalization ratio to approx. 20 %, indicating a specific interaction between this linker part and PSMA. Compound **8** was not considered for further evaluation due to its low internalization ratio. However, compound **9** bearing two non-natural β-sulfoalanines also showed similarly high internalization ratio as compound **5**. Overall the results from this set were quite surprising for us. Initially we expected that the hydrophilic linker B would bend towards the less rigid outlet of the entrance funnel of the PSMA protein as observed for the DOTA chelator in PSMA-617 (see Figure 5 in reference 7) and that the positive effect of the two glutamic acids in compound **5** on the internalization ratio would be rather unspecific. While the lower internalization ratio of compound **7** seems to contradict this, our expectation would be in line with the behavior of compound **9**. Further investigations with the mixed DGlu-LGlu and LGlu-DGlu in linker B and replacement of the glutamic acids by aspartic acids might help to elucidate this effect. However, we also had the opportunity to investigate this effects using protein crystallography. Thus, compounds **5**, **7** and **9** were co-crystallized with PSMA and analyzed using x-ray crystallography (see below).

Crystal Structures of PSMA with Compounds 5, 7, and 9. The structural data presented above was not in line with our expectation and expands our understanding of interaction pattern governing inhibitor recognition by PSMA emphasizing the importance of flexibility of the enzyme

to accommodate diverse inhibitory scaffolds. Furthermore, it brings about the call for caution when interpreting SAR data and modeling inhibitor binding modes, as even minor modifications in the inhibitor molecule can have a profound effect on its interactions with PSMA.[38] The latter fact is documented by the comparison of **5** and **7**, two stereoisomers differing only in the stereochemistry of glutamates of the linker B. Despite the fact that none of the glutamate moieties is engaged in PSMA interactions and cannot thus efficiently guide the terminal label group to a defined position within the structure, the "linker B-label" parts of the two inhibitors occupy spatially distinct positions, with the terminal fluorine atoms more than 21 Å apart (Figure 4).

Interestingly, the terminal fluoro-pyridine label of **5** is inserted into the arene-binding site of PSMA. This binding mode thus expands a collection of PSMA inhibitors and natural substrates exploiting this shallow binding cleft at the surface of the enzyme.[19,39,40] It shall be noted that in previous studies, the engagement of the ABS by a terminal inhibitor group resulted in substantial, up to 60-fold, increase in their binding affinity for PSMA.[37] However, no such affinity enhancement was observed for **5**, as its *in vitro* inhibition constant is comparable to **7**, the terminal label of which does not interact with residues forming the ABS. Obviously, at least in the case of *in vitro* affinity measurements, the ABS engagement by the inhibitor is not necessarily directly linked to the increase of affinity in all cases as additional inhibitor characteristics that are not directly quantifiable by biochemical/structural experiments (e.g. inhibitor solvation, deformation energy upon binding) may influence overall binding energy.

Our structural data also underscores the importance of the flexibility of the entrance lid (amino acids Trp541-Gly548) to accommodate inhibitors with bulky distal parts.[41] It shall be noted that binding of **5** is accompanied by the substantial repositioning of the lid to accommodate the inhibitor (Figure 6). This rearrangement is necessary to avoid steric clashes between PSMA side

chains and the inhibitor. More importantly, the repositioning of the lid results in the relocation of the Trp541 side chain by 4.1 Å and the formation of the "open" ABS that can be then engaged by the inhibitor (Figure 6). Considering this special binding mode together with the almost complete localization of compound **5** within the PSMA binding pocket one could define the complete molecule as an extended binding motif compared to the well-known Glu-Urea-Lys. In combination with the results from the *in vitro* and *in vivo* evaluation this almost perfect interaction with the PSMA settled our choice of compound **5** for clinical translation.

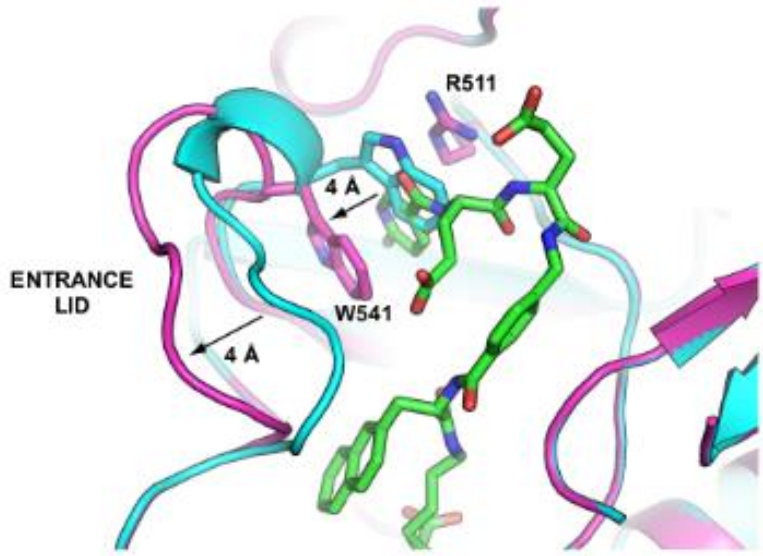

Figure 6. Positional flexibility of the entrance lid (amino acids W541-G548) is critical for the formation of the arene-binding site upon inhibitor binding. Superposition of PSMA complexes with compound **5** (PSMA purple, compound **5** green, PDB-ID: 5O5U) and compound **7** (PSMA cyan; compound **7** inhibitor omitted for clarity, only PSMA part of complex visualized, PDB-ID 5O5R). The protein is shown in cartoon representation and compound **5** in stick representation. Notice 4 Å movement of the entrance lid upon compound **5** binding leading to the formation of the arene-binding site.

Compound Set IV. In this set, the influence of linker A was reinvestigated while linker B was consisting of two glutamic acids, as for compound **5**. While the binding affinity of compounds **10** and **11** towards PSMA was in the typical range, the affinity of compound **12** was very low. The former two compounds showed both comparatively low internalization ratios. This was especially unexpected for compound **10**, since this compound is structurally most similar to PSMA-617 of all compounds investigated in this study. The internalization of compound **12** was not investigated due to its low binding affinity. This drop of affinity was also observed for other compounds with positive charges in this area of the linker (unpublished data), and might be caused by a negative interaction with the arginine patch of the PSMA.[7] However, further studies would be necessary to verify this. Since none of the compounds matched the *in vitro* characteristics of compound **5** a further evaluation of the compounds of this set was not considered. Albeit we would not expect a similar good interaction with the PSMA protein, a crystal structure of PSMA with compound **10** would be interesting closing the gap between PSMA-617 and compound **5** (PSMA-1007).

Summary and conclusion. In the present work, we have summarized the *in vitro* characterization of several compounds developed during our search for a suitable, ^{18}F-labeled PSMA ligand. Backed up by early *in vivo* experiments, compound **5**, better known as PSMA-1007 – or [^{18}F]PSMA-1007 in its radiolabeled form – was selected as lead candidate for clinical application in the PET imaging of prostate cancer. Reinvestigation of the lipophilic and hydrophilic areas of the linker by *in vitro* cell binding experiments confirmed our selection. These results were further supported by co-crystallization experiments with the PSMA protein itself, revealing that compound **5** fully engages known inhibitor interacting motifs. In the meantime,

[^{18}F]PSMA-1007 has successfully passed clinical translation and is a promising subject in ongoing clinical trials as new tool for the detection and stratification of prostate cancer.[29,42,43]

Experimental Section

General. All solvents and reagents were purchased from Sigma-Aldrich (Taufkirchen, Germany), VWR (Bruchsal, Germany), Iris Biotech (Marktredwitz, Germany), Bachem (Bubendorf, Switzerland) and Carl Roth (Karlsruhe, Germany), were at least of synthesis grade and used without further purification if not stated otherwise. Mass spectra were recorded on a Bruker microflex LRF system. HPLC analyses were performed on an Ultimate 3000 system with a variable wavelength detector RS 3000 (both Thermo Fisher Scientific, Schwerte, Germany) and a Gabi detector (Raytest, Straubenhardt, Germany) for radioactivity detection, equipped with a Chromolith performance C18ec 100 4.6-mm column (Merck, Darmstadt, Germany). For Semipreparative runs the system was equipped with a Chromolith® RP-18ec 100-10 mm column (Merck, Darmstadt, Germany). The system was controlled by Chromeleon software version 7.1.2 (Thermo Fisher Scientific, Schwerte, Germany).

Synthesis and characterization of labeling precursors and reference compounds. The peptidomimetic precursors and reference compounds were synthesized by manual solid-phase synthesis using standard Fmoc-chemistry as published earlier.[44,45] Briefly, the binding motif Glu-Urea-Lys was built up from resin bound lysine (side chain protected with Alloc) and the *bis t*-Bu protected isocyanate of glutamic acid (10 Eq, generated *in situ* from H-(*t*-Bu)Glu(*t*-Bu) and triphosgene in DCM in presence of excess DIPEA).[16] Subsequently, the linker was synthesized by standard Fmoc solid phase chemistry (4 eq. natural or non-natural amino acid activated with HBTU {0.98 eq. with respect to the amino acid} for 2 minutes).[11] For the synthesis of the reference

compounds, half of the resin was further coupled to activated 6-fluoronicotinic acid while the second half was designated as labeling precursor.[13] Cleavage from the resin was achieved using TFA/TIS/H_2O (95:2.5:2.5) and the products were purified by semipreparative HPLC. Reaction conditions were not optimized and yields were not determined. The purity was checked by HPLC and was at least 95 % for all compounds. The identity of all compounds was confirmed by MALDI-MS. The respective results are summarized in Table 3.

Table 3. Results of the identification of compounds 1-12 and the respective labeling precursors by MALDI-MS

Compound*	Sum formula	$[M+H^+]^+$ (calc.)	$[M+H^+]^+$ (found)
1	$C_{39}H_{47}FN_6O_{10}$	779.34	779.7
P1	$C_{33}H_{45}N_5O_9$	656.33	656.3
2	$C_{31}H_{34}FN_5O_9$	640.24	640.4
P2	$C_{25}H_{32}N_4O_8$	517.23	517.1
3	$C_{39}H_{41}FN_5O_{10}$	773.29	773.3
P3	$C_{33}H_{39}N_4O_9$	650.28	650.3
4	$C_{44}H_{48}FN_7O_{13}$	902.34	902.5
P4	$C_{38}H_{46}N_6O_{12}$	779.33	779.4
5	$C_{49}H_{55}FN_8O_{16}$	1031.38	1032.1
P5	$C_{43}H_{53}N_7O_{15}$	908.37	908.7
6	$C_{54}H_{62}FN_9O_{19}$	1160.42	1160.8
P6	$C_{48}H_{60}N_8O_{18}$	1037.41	1037.6
7	$C_{49}H_{55}FN_8O_{16}$	1031.38	1031.8
P7	$C_{43}H_{53}N_7O_{15}$	908.37	907.8
8	$C_{42}H_{46}FN_7O_{14}S$	924.29	924.7

P8	$C_{36}H_{44}N_6O_{13}S$	801.21	801.8
9	$C_{45}H_{51}FN_8O_{18}S_2$	1075.28	1075.8
P9	$C_{39}H_{49}N_7O_{17}S_2$	952.27	952.7
10	$C_{49}H_{61}FN_8O_{16}$	1037.43	1037.7
P10	$C_{43}H_{59}N_7O_{15}$	914.41	914.4
11	$C_{46}H_{55}FN_8O_{18}$	1027.37	1027.9
P11	$C_{40}H_{53}N_7O_{17}$	904.36	904.9
12	$C_{48}H_{60}FN_9O_{16}$	1038.42	1038.7
P12	$C_{42}H_{58}N_8O_{15}$	915.41	915.7

*** PX** is the precursor for the radiosynthesis of the ligand **[^{18}F]X** corresponding to compound **X** (with **X** = **1-12**) by reaction with [^{18}F]F-Py-TFP (Scheme 2).

Radiolabeling. Production and activation of [^{18}F]fluoride, as well as radiosynthesis of 6-[^{18}F]F-Py-TFP and subsequent coupling to **[^{18}F]1-4** was accomplished as reported earlier.[13] Briefly, 6-[^{18}F]F-Py-TFP was prepared by direct nucleophilic substitution on the corresponding trimethylammonium triflate precursor.[12,13] Subsequently, 6-[^{18}F]F-Py-TFP was isolated by solid phase extraction, eluted in 65:35 MeCN:H_2O and coupled to **P1**-**P4** under phosphate buffered aqueous conditions. For the synthesis of **[^{18}F]5-12** a modification of the elution procedure for the prosthetic group 6-[^{18}F]F-Py-TFP was applied: after the washing step with 10 ml water, the MCX cartridge (Oasis) was dried using 20-40 ml air and the cartridge rinsed with 500 µl dry acetonitrile. Subsequently, the product was eluted *via* a SepPak SodSulf drying cartridge (Waters) using 0.8-1.2 ml of dry acetonitrile. For the following coupling reactions, 200 µl of the (dry) 6-[^{18}F]F-Py-TFP solution were mixed with 50 µl of the respective precursor and 10 µl of DIPEA. Then, the mixture was heated at 60 °C for 20-50 minutes* and the labeled product separated by semipreparative HPLC. Using this procedure, up to four labeled ligands could be synthesized in

parallel. Reaction conditions were not optimized. The radiochemical yields are summarized in Table 4. The radiochemical purity of the ligands was at least 98 % after separation by semi-preparative HPLC. Identification of the labeled products was confirmed using analytical HPLC by co-elution with the respective, non-radioactive standard ("co-elution" in the radio HPLC).

*Usually up to four different radioligands were produced in parallel for direct comparison of the internalization rate. Since the separation by semipreparative HPLC had to be conducted after each other, the pending reactions were left in the heating block resulting in the variable reaction time.

Table 4. Summary of the results from the radiolabeling experiments

Compound	t_{ret} [min] (Gradient)	RCY [%]
[^{18}F]**1**	5.02 (1)	26±4
[^{18}F]**2**	4.79 (1)	16±1
[^{18}F]**3**	5.09 (1)	36±3
[^{18}F]**4**	6.48 (2)	11 ±3
[^{18}F]**5**	4.56 (1)	26±9*
[^{18}F]**6**	3.87 (3)	20±6*
[^{18}F]**7**	3.87 (2)	29±6*
[^{18}F]**8**	4.03 (1)	57±9*
[^{18}F]**9**	3.10 (3)	62±7*
[^{18}F]**10**	4.43 (1)	47±7*
[^{18}F]**11**	6.48 (3)	60±7*
[^{18}F]**12**	3.22 (3)	-

RCY determined with respect to 6-[^{18}F]F-Py-TFP; Gradients: Solvent A: acetonitrile; Solvent B: 0.1 % TFA in H_2O; A + B = 100 %; Gradient 1: 5 % A to 95 % A in 12.5 minutes; Gradient 2: 5 % A to 50 % A in 10 minutes; Gradient 3: 5 % A to 95 % A in 10 minutes; Flow: 3 ml/min each; column: Chromolith performance RP 18 ec 4.6X100 mm; dead time 0.56 minutes each (thiourea)

Formulation. For the formulation of each ligand, the HPLC-fraction containing the respective product was diluted with water (approx. 10 ml), concentrated on a pre-conditioned (5 ml MeOH followed by 10 ml H_2O) SepPak C-18 light cartridge (Waters) and eluted in 1 ml ethanol/water (70:30 v/v). The solvent was evaporated at 98 °C under a stream of air and the dry residue (invisible tracer amounts) dissolved in a 6 µM solution of the respective reference compound in 0.9 % NaCl so that an activity concentration of approx. 100 MBq/ml was reached. Finally, the identity of the products was confirmed by analytical radio-HPLC and comparison (radioactivity- and UV-channel) with the non-radioactive reference compounds (co-elution). For small animal PET and organ distribution experiments the dry tracer was dissolved in a minimum amount of saline (100-200 µl) and the molar activity was determined by HPLC before final formulation. Then the solution was diluted with 0.9 % NaCl to a 0.6 µmolar concentration of the tracer with an activity concentration of approx. 100-250 MBq/ml (small animal PET) or 10-20 MBq/ml (organ distribution; further dilution with 0.6 µmolar solution of the respective non-labeled reference compound).

Crystallization and data collection Diffraction quality crystals were grown using the hanging-drop vapor diffusion method at 293 K according to the established protocol.[46] Briefly, PSMA (9 mg/ml) was mixed with a 10 mM solution of given inhibitor dissolved in 50 mM Tris-HCl, 150 mM NaCl, pH 8.0, at 9:1 (v/v) ratio. Protein/inhibitor solution was then mixed with the equal volume of mother liquor [33% (v/v) pentaerythritol propoxylate PO/OH 5/4 (Sigma Aldrich), 2 % (w/v) PEG 3350, and 100 mM Tris-HCl, pH 8.0] and 1 µl crystallization droplets equilibrated against 800 µl of the mother liquor. Orthorhombic crystals (I222, a = 101 Å, b = 130 Å, c = 159 Å) were vitrified in liquid nitrogen directly from crystallization droplets. Diffraction data were collected from a single crystal using synchrotron radiation at the MX 14.1 beamline (0.91841 Å;

BESSYII, Berlin, Germany) at 90K. (5O5R, 5O5U) and at the MX1 Beamline 13 (0.9796 Å, DESY, Hamburg, Germany) at 100 K (5O5T). Both beamlines are equipped with Pilatus 6M detector (Dectris, Switzerland). Datasets were indexed, integrated and scaled using the XDSAPP interface.[47]

Structure refinement. Difference Fourier methods were used to determine structures of PSMA/inhibitor complexes with ligand-free PSMA (PDB code 2OOT) used as a starting model. Iterative refinement and model building cycles were performed using Refmac 5.5. and *Coot*, respectively.[48,49] Ligand topologies and coordinates were generated with *PRODRG* and inhibitors were fitted into $|F_o| - |F_c|$ electron density maps in the final stages of the refinement.[50] Approximately 1,000 randomly selected reflections were kept aside for cross-validation (R_{free}) during the refinement process. The final models were validated using the *MolProbity* server[51] and deposited in the Protein Data Bank (PDB) under accession codes 5O5T (compound **5**), 5O5R (compound **7**), and 5O5U (compound **9**). The data collection and structure refinement statistics are summarized in Table 5 below.

Table 5: Data collection and refinement statistics

Data collection statistics			
Inhibitor	Compound **5**	Compound **7**	Compound **9**
PDB code	5O5T	5O5R	5O5U
Wavelength (Å)	0.9796	0.9184	0.9184
Space group	23 (I222)	23 (I222)	23 (I222)
Unit-cell parameters *a, b, c* (Å)	101.66, 130.16, 159.16	101.51, 130.20, 159.16	101.79, 130.41, 159.10
Resolution limits (Å)	45.38 – 1.43 (1.45 – 1.43)	49.13 – 1.65 (1.68 – 1.65)	49.13 – 1.53 (1.55 – 1.53)

Number of unique reflections	183216 (7062)	125247 (5979)	157677 (7245)
Redundancy	5.1 (3.7)	4.5 (4.6)	5.2 (5.2)
Completeness (%)	95.2 (74.9)	99.1 (96.4)	99.1 (92.7)
$I/\sigma I$	23.6 (1.7)	15.4 (1.7)	13.7 (1.8)
R_{merge}	0.032 (0.656)	0.055 (0.953)	0.053 (0.948)
Refinement Statistics			
Resolution limits (Å)	50.00 - 1.43 (1.47 - 1.43)	50.00 – 1.65 (1.69 – 1.65)	29.57 – 1.53 (1.57-1.53)
Total number of reflections	177614 (10818)	118929 (8635)	154553 (11133)
Number of reflections in working set	17212 (10465)	112616 (8175)	151450(10910)
Number of reflections in test set	5602 (353)	6313 (460)	3103 (223)
R/R_{free} (%)	13.8/17.3 (28.6/30.0)	16.1/18.55 (27.7/28.8)	16.4/18.0 (29.1/32.9)
Total number of non-H atoms	6676	7020	6910
Number of non-H protein atoms	5810	6081	5927
Number Inhibitor molecules	74	74	74
Number of water molecules	603	625	617
Average B-factor (Å^2)	32.8	37.5	33.8
Protein atoms	31.3	35.5	31.2
Waters	43.0	46.5	41.8
Inhibitor	27.5	60.6	53.8
[&]Ramachandran Plot (%)			
Most favored	97	97	98
Additionally allowed	3	2	2
Disallowed	Val 382, Gly 335	(LysA 655, Val 382, Phe 653)	Ser 656, Val 382)
R.m.s. deviations: bond lengths (Å)	0.019	0.018	0.017

bond angles (°)	1.83	1.85	1.78
planarity (Å)	0.011	0.011	0.011
chiral centers (Å^3)	0.17	0.13	0.12
Missing residues	AA 44-54	AA 44-54	AA 44-54

* Values in parenthesis are for the highest resolution shells.

& Structures were analyzed using the MolProbity 4.02b-467

Preclinical evaluation, General. Preclinical evaluation was conducted according to previously published procedures.[13] All animal experiments were conducted in compliance with the current laws of the Federal Republic of Germany. For *in vivo* and organ distribution experiments, 8 week old male athymic BALB/c nu/nu mice were subcutaneously inoculated into the right trunk with 5 x 10^6 LNCaP cells in 50% Matrigel. The organ distribution studies were carried out when the tumor size was approximately 1 cm^3.

Cell Culture. For binding studies and *in vivo* experiments, LNCaP cells (metastatic lesion of human prostatic adenocarcinoma, ATCC® CRL-1740™) were cultured in RPMI 1640 (PAN Biotech) medium supplemented with 10% fetal calf serum and stabilized glutamine (PAN Biotech). Cells were grown at 37 °C in an incubator with humidified air, equilibrated with 5 % CO_2.

Determination of the Binding Affinity. The competitive cell binding assays and internalization experiments were performed as described previously.[13] Briefly, LNCaP cells (10^5 per well) were incubated with the ^{68}Ga-labeled radioligand [Glu-urea-Lys(Ahx)]$_2$-[^{68}Ga(HBED-CC)] (^{68}Ga-PSMA-10)[52] at a concentration of 0.75 nM in the presence of 12 different concentrations of the (unlabeled) compounds **1-12** (0–5000 nM, 100 µl/well). After incubation, washing was carried out using a multiscreen vacuum manifold (Millipore, Billerica, MA). Cell-bound radioactivity was measured using a gamma counter (Packard Cobra II, GMI, Minnesota, USA). The 50 % inhibitory

concentrations (IC_{50}) were calculated by fitting the data using a nonlinear regression algorithm (GraphPad Prism 5.01 Software). Experiments were performed as quadruplicate.

Determination of Cellular Binding / Uptake. To determine the specific cell uptake and internalization, 10^5 cells were seeded in poly-L-lysine coated 24-well cell culture plates for 24 h. The cells in each well were incubated with 250 µl of a 30 nM solution of the respective c.a. radioligand (**[18F]1-12**; 15-20 GBq/µmol) in Opti-MEM I medium (Gibco). Specific cellular uptake was determined by blocking with 2-(phosphonomethyl)pentanedioic acid (2-PMPA) (500 µM final concentration, Axxora, Loerrach, Germany). All experiments were conducted at 37 °C and 4 °C. The incubation was terminated after 45 min by washing 3 times with 1 ml of ice-cold phosphate buffered saline. The cells were subsequently incubated twice with 0.5 ml glycine-HCl (50 mM, pH = 2.8) for 5 min each to remove the surface-bound fraction; the supernatant was collected. After an additional washing step with 1 ml ice-cold phosphate buffered saline, the cells were lysed using 0.5 ml NaOH (0.3 N), collected and measured in a gamma counter. The specific cellular uptake was calculated as percent of the initially added radioactivity bound to 10^5 cells %IA/10^5 cells by subtraction of the respective uptake under blocking conditions. All experiments were conducted as triplicate.

Small animal PET. For the small animal PET study 100 µl 0.6 µM of the respective c.a. radioligand (**[^{18}F]3** or **[^{18}F]5**; approx. 420 GBq/µmol; 60 pmol; 25 MBq; approx. 100 µl) were injected via a lateral tail vein into a mouse bearing an LNCaP tumor xenograft. The anaesthetized animal (2% sevoflurane, Abbott, Wiesbaden, Germany) was placed in prone position into the Inveon small animal PET scanner (Siemens, Knoxville, Tenn., USA) to perform a dynamic small animal PET scan. Prior to the scan the transmission was measured for 900 s using a rotating Co-57 source. Acquisition was started 3 s before the tracer was injected and continued for 3600 s in

list mode. The radial field of view was 7.5 cm. A second scan was performed 2 h p.i.. Between the first and the second scan the mouse was allowed to wake up.

The scans were reconstructed using the software Acquisition Workplace (Siemens) with a 28 frame protocol (2 times 15 s, 8 times 30 s, 5 times 60 s, 5 times 120 s, 8 times 300 s). The volumes of interest for the generation of the time-activity-curves were drawn manually over the respective organs. Reconstruction of the images was done with the OSEM 3D MAP algorithm (MAP iterations: 18, output interval: 20; Image x-y size 256, image z size 161; size of voxel: x,y: 0.43 mm, z: 0.796 mm).

Organ Distribution. Organ distribution studies were carried out with mice bearing LNCaP tumors (n = 3). The compound (**3** or **5**) was administered as 0.6 µM solution (100 µl; 60 pmol), spiked with 1-2 MBq of the respective radioligand (**[^{18}F]3** or **[^{18}F]5**) via tail vein injection. At 1 h p. i., the animals were sacrificed (CO_2 asphyxiation), organs of interest were dissected, blotted dry and weighed. The radioactivity was measured with a gamma counter (Packard Cobra II, GMI, Minnesota, USA) and calculated as % ID/g.

ASSOCIATED CONTENT

The corresponding time-activity-curves from the PET experiments as well as (radio)chromatograms (HPLC) of key components are summarized in the supporting information jm-2019-01479m-SI.docx. Molecular formular strings (MFS) of all presented substances are summarized in the file jm-2019-01479m-MFS.csv.

Accession Codes

PDB code for PSMA with bound **5** is 5O5T

PDB code for PSMA with bound **7** is 5O5R

PDB code for PSMA with bound **9** is 5O5U

AUTHOR INFORMATION

Corresponding Author

*E-mail: Cardinale81@web.de.

Present Addresses

Department of Nuclear Medicine, University Hospital Heidelberg, INF 400, 69239 Heidelberg, Germany.

⊥Universitatsklinikum Freiburg, Department of Nuclear Medicine, Hugstetter Strasse 55, 79106 Freiburg, Germany.

∥ Helmholtz-Zentrum Dresden-Rossendorf e.V. (HZDR), Institute of Radiopharmaceutical Cancer Research, Bautzner Landstraße 400, 01328 Dresden, Germany.

Author Contributions

The manuscript was written through contributions of all authors. All authors have given approval to the final version of the manuscript.

Funding Sources

This project was supported by a postdoctoral scholarship from ABX Advanced Biochemical Compounds GmbH (DKFZ file no. L-15309). We acknowledge Helmholtz-Zentrum Berlin for the allocation of synchrotron radiation beamtime at the MX14.1 beamline and funding from the

European Community´s Seventh Framework Programme (FP7/2007-2013) under a BioStruct-X (grant agreement N°28 3570). The synchrotron MX1 data was collected at the P13 beamline operated by EMBL Hamburg at the PETRA III storage ring (DESY, Hamburg, Germany). Additionally, this work was in part supported by the CAS (RVO: 86652036), the Czech Science Foundation (18-04790S), and project BIOCEV (CZ.1.05/1.1.00/02.0109) from the ERDF. Finally, this work was partly funded by a grant of the Federal Ministry of Education and Research (BMBF), project ProstaPET (2U2WTZKOREA-021; no. 01DR17031A).

Notes

[^{18}F]PSMA-1007 is the subject of a patent application by Jens Cardinale, Martin Schäfer, Martina Benešová, Ulrike Bauder-Wüst, Matthias Eder, Uwe Haberkorn, Frederik Giesel, and Klaus Kopka. No other potential conflict of interest relevant to this article was reported.

ACKNOWLEDGMENT

We thank Karin Leotta, Oksana Hautzinger and Uschi Schierbaum for their support regarding organ distribution and small animal PET experiments.

Abbreviations Used

ABS, arene binding site; Alloc, allyloxycarbonyl; DIPEA, diisopropylethylamine; DOTA, 1,4,7,10-Tetraazacyclododecane-1,4,7,10-tetraacetic acid; HBTU, 3-[Bis(dimethylamino)methyliumyl]-3H-benzotriazol-1-oxide hexafluorophosphate; LNCaP, metastatic prostate cancer cells derived from left supraclavicular lymph node; MFS, molecular formula strings; MIP, maximum intensity projection; OSEM, ordered subset expectation maximization; PSA, prostate specific antigene; PSMA, prostate specific membrane antigene; RCY, radiochemical yield; RPMI; SUV, standartized uptake value; TIS, triisoprypylsilane.

REFERENCES

(1) Afshar-Oromieh, A.; Haberkorn, U.; Eder, M.; Eisenhut, M.; Zechmann C. M. [^{68}Ga]Gallium-Labelled PSMA Ligand as Superior PET Tracer for the Diagnosis of Prostate Cancer: Comparison with ^{18}F-FECH. *Eur. J. Nucl. Med. Mol. Imaging* **2012**, *39*, 1085-1086.

(2) Schwenck. J.; Rempp, H.; Reischl, G.; Kruck, S.; Stenzl, A.; Nikolaou, K.; Pfannenberg, C.; la Fougère, C. Comparison of ^{68}Ga-Labelled PSMA-11 and ^{11}C-Choline in the Detection of Prostate Cancer Metastases by PET/CT. *Eur. J. Nucl. Med. Mol. Imaging* **2017**, *44*, 92-101.

(3) Afshar-Oromieh, A.; Zechmann, C. M.; Malcher, A.; Eder, M.; Eisenhut, M.; Linhart, H. G.; Holland-Letz, T.; Hadaschik, B. A.; Giesel, F. L.; Debus, J.; Haberkorn, U. Comparison of PET Imaging with a ^{68}Ga-Labelled PSMA Ligand and ^{18}F-Choline-Based PET/CT for the Diagnosis of Recurrent Prostate Cancer. *Eur. J. Nucl. Med. Mol. Imaging* **2014**, *41*, 11-20.

(4) Evangelista, L.; Briganti, A.; Fanti, S.; Joniau, S.; Reske, S.; Schiavina, R.; Stief, C.; Thalmann, G. N.; Picchio, M. New Clinical Indications for ^{18}F/^{11}C-choline, New Tracers for Positron Emission Tomography and a Promising Hybrid Device for Prostate Cancer Staging: A Systematic Review of the Literature. *Eur. Urol.* **2016**, *70*, 161-175.

(5) Oliveira, J. M.; Gomes, C.; Faria, D. B.; Vieira, T. S.; Silva, F. A.; Vale, J.; Pimentel, F. L. ^{68}Ga-Prostate-Specific Membrane Antigen Positron Emission Tomography/Computed Tomography for Prostate Cancer Imaging: A Narrative Literature Review. *World J. Nucl. Med.* **2017**, *16*, 3-7.

(6) Pfister, D.; Porres, D.; Heidenreich, A.; Heidegger, I.; Knuechel, R.; Steib, F.; Behrendt, F. F.; Verburg, F. A. Detection of Recurrent Prostate Cancer Lesions Before Salvage

Lymphadenectomy is more Accurate with ^{68}Ga-PSMA-HBED-CC than with ^{18}F-Fluoroethylcholine PET/CT. *Eur. J. Nucl. Med. Mol. Imaging* **2016**, *43*, 1410-1417.

(7) Kopka, K.; Benešová, M.; Bařinka, C.; Haberkorn, U.; Babich, J. Glu-Ureido-Based Inhibitors of Prostate-Specific Membrane Antigen: Lessons Learned During the Development of a Novel Class of Low-Molecular-Weight Theranostic Radiotracers. *J. Nucl. Med.* **2017**, *58*(Suppl 2), 17S-26S.

(8) Afshar-Oromieh, A.; Holland-Letz, T.; Giesel, FL.; Kratochwil, C.; Mier, W.; Haufe, S.; Debus, N.; Eder, M.; Eisenhut, M.; Schäfer, M.; Neels, O.; Hohenfellner, M.; Kopka, K.; Kauczor, HU.; Debus, J.; Haberkorn, U. Diagnostic Performance of 68Ga-PSMA-11 (HBED-CC) PET/CT in Patients with Recurrent Prostate Cancer: Evaluation in 1007 Patients. *Eur. J. Nucl. Med. Mol. Imaging* **2017**, *44*, 1258-1268.

(9) Will, L.; Sonni, I.; Kopka, K.; Kratochwil, C.; Giesel, FL.; Haberkorn, U. Radiolabeled Prostate-Specific Membrane Antigen Small-Molecule Inhibitors. *Q. J. Nucl. Med. Mol. Imaging* **2017**, *61*, 168-180.

(10) Afshar-Oromieh, A.; Babich, JW.; Kratochwil, C.; Giesel, FL.; Eisenhut, M.; Kopka, K.; Haberkorn, U. The Rise of PSMA Ligands for Diagnosis and Therapy of Prostate Cancer. *J. Nucl. Med.* **2016**, *57*(Suppl 3), 79S-89S.

(11) Calais, J.; Fendler, PF.; Herrmann, K.; Eiber, M.; Ceci, M. Comparison of ^{68}Ga-PSMA-11 and ^{18}F-Fluciclovine PET/CT in a Case Series of 10 Patients with Prostate Cancer Recurrence: Interesting, but Far from Definitive. *J. Nucl. Med.* **2018**, *59*, 789-794.

(12) Calais, J.; Ceci, F.; Nguyen, K.; Gartmann, J.; Matthias Eiber, M.; Reiter, RE.; Kishan, A. U.; Hossein Jadvar, H.; Fendler, W. P.; Czernin, J. Prospective Head-to-Head Comparison of 18F-Fluciclovine and 68Ga-PSMA-11 PET/CT for Localization of Prostate Cancer Biochemical Recurrence After Primary Prostatectomy. *J. Clin. Oncology* **2019**, *37*, Suppl 15.

(13) Eder, M.; Neels, O.; Müller, M.; Bauder-Wüst, U.; Remde, Y.; Schäfer, M.; Hennrich, U.; Eisenhut, M.; Afshar-Oromieh, A.; Haberkorn, U.; Kopka, K. Novel Preclinical and Radiopharmaceutical Aspects of [^{68}Ga]Ga-PSMA-HBED-CC: A New PET Tracer for Imaging of Prostate Cancer. *Pharmaceuticals (Basel)* **2014**, *7*, 779-796.

(14) Afshar-Oromieh, A.; Hetzheim, H.; Kratochwil, C.; Benesova, M.; Eder, M.; Neels, O. C.; Eisenhut, M.; Kübler, W.; Holland-Letz, T.; Giesel, F. L.; Mier, W.; Kopka, K.; Haberkorn, U. The Theranostic PSMA Ligand PSMA-617 in the Diagnosis of Prostate Cancer by PET/CT: Biodistribution in Humans, Radiation Dosimetry, and First Evaluation of Tumor Lesions. *J. Nucl. Med.* **2015**, *56*, 1697-1705.

(15) Weineisen, M.; Schottelius, M.; Simecek, J.; Baum, R. P.; Yildiz, A.; Beykan, S.; Kulkarni, H. R.; Lassmann, M.; Klette, I.; Eiber, M.; Schwaiger, M.; Wester, H. J. ^{68}Ga- and ^{177}Lu-Labeled PSMA I&T: Optimization of a PSMA-Targeted Theranostic Concept and First Proof-of-Concept Human Studies. *J. Nucl. Med.* **2015**, *56*, 1169-1176.

(16) Ceci, F.; Castellucci, P.; Fanti S. Current Application and Future Perspectives of Prostate Specific Membrane Antigen PET Imaging in Prostate Cancer. *Q. J. Nucl. Med. Mol. Imaging* **2019**, *63*, 7-18.

(17) Zippel. C.; Neels. OC.; Hennrich. U.; Giesel. FL.; Kopka. K. [Initiation of Clinical Multicentre Studies with Local Radiotracer Production - Regulatory Environment and Radiopharmaceutical-Organisational Aspects]. *Nuklearmedizin* **2019**, *58*, 77-85.

(18) De Visschere, PJL.; Standaert, C.; Fütterer, JJ.; Villeirs, GM.; Panebianco, V.; Walz, J.; Maurer, T.; Hadaschik, BA.; Lecouvet, FE.; Giannarini, G.; Fanti, S. A Systematic Review on the Role of Imaging in Early Recurrent Prostate Cancer. *Eur. Urol. Oncol.* **2019**, *2*, 47-76.

(19) Benešová, M.; Schäfer, M.; Bauder-Wüst, U.; Afshar-Oromieh, A.; Kratochwil, C.; Mier, W.; Haberkorn, U.; Kopka, K.; Eder, M. Preclinical Evaluation of a Tailor-Made DOTA-Conjugated PSMA Inhibitor with Optimized Linker Moiety for Imaging and Endoradiotherapy of Prostate Cancer. *J. Nucl. Med.* **2015**, *56*, 914-920.

(20) Benešová, M.; Bauder-Wüst, U.; Schäfer, M.; Klika, K. D.; Mier, W.; Haberkorn, U.; Kopka, K.; Eder, M. Linker Modification Strategies to Control the Prostate-Specific Membrane Antigen (PSMA)-Targeting and Pharmacokinetic Properties of DOTA-Conjugated PSMA Inhibitors. *J. Med. Chem.* **2016**, *59*, 1761-1775.

(21) Hofman, M. S.; Violet, J.; Hicks, R. J.; Ferdinandus, J.; Thang, S. P.; Akhurst, T.; Iravani, A.; Kong, G.; Kumar, A. R.; Murphy, D. G.; Eu, P.; Jackson, P.; Scalzo, M.; Williams, S. G.; Sandhu, S. [^{177}Lu]-PSMA-617 Radionuclide Treatment in Patients with Metastatic Castration-Resistant Prostate Cancer (LuPSMA Trial): A Single-Centre, Single-Arm, Phase 2 Trial. *Lancet Oncol*. **2018**, *19*, 825-833.

(22) Kratochwil, C.; Bruchertseifer, F.; Giesel, F. L.; Weis, M.; Verburg, F. A.; Mottarghy, F.; Kopka, K.; Apostolidis, C.; Haberkorn, U.; Morgenstern, A. ^{225}Ac-PSMA-617 for PSMA-

562 Targeted α-Radiation Therapy of Metastatic Castration-Resistant Prostate Cancer. *J. Nucl. Med.*
563 **2016**, *57*, 1941-1944.

564 (23) Cardinale, J.; Schäfer, M.; Benesova, M.; Bauder-Wüst, U.; Komljenovic, D.; Eder, M.;
565 Ladd, M. E.; Kopka, K. OP426: Radiosyntheses and Preclinical Evaluation of Radiofluorinated
566 PSMA-Ligands. *Eur. J. Nucl. Med. Mol. Imaging* **2015**, *42*, S173.

567 (24) Cardinale, J.; Schäfer, M.; Geerlings, M.; Benešová, M.; Eder, M.; Bauder-Wüst, U.;
568 Baranski, A.; Neels, O.; Leotta, K.; Haberkorn, U.; Giesel, F.; Kopka, K. OP022: ^{18}F-PSMA-1007:
569 The Optimal Variant of Radiofluorinated PSMA Ligands Derived from PSMA-617. *Eur. J. Nucl.*
570 *Med. Mol. Imaging* **2016**, *43*, S14.

571 (25) Cardinale, J.; Schäfer, M.; Benešová, M.; Bauder-Wüst, U.; Leotta, K.; Eder, M.; Neels,
572 O. C.; Haberkorn, U.; Giesel, F. L.; Kopka, K. Preclinical Evaluation of ^{18}F-PSMA-1007, a New
573 Prostate-Specific Membrane Antigen Ligand for Prostate Cancer Imaging. *J. Nucl. Med.* **2017**, *58*,
574 425-431.

575 (26) Giesel, F. L.; Hadaschik, B.; Cardinale, J; Radtke, J.; Vinsensia, M.; Lehnert, W.; Kesch,
576 C.; Tolstov, Y.; Singer, S.; Grabe, N.; Duensing, S.; Schäfer, M.; Neels, O. C.; Mier, W.;
577 Haberkorn, U.; Kopka, K.; Kratochwil, C. F-18 Labelled PSMA-1007: Biodistribution, Radiation
578 Dosimetry and Histopathological Validation of Tumor Lesions in Prostate Cancer Patients. *Eur.*
579 *J. Nucl. Med. Mol. Imaging* **2017**, *44*, 678-688.

580 (27) Giesel, F. L.; Kesch, C.; Yun, M.; Cardinale, J.; Haberkorn, U.; Kopka, K.; Kratochwil, C.;
581 Hadaschik, B. A. 18F-PSMA-1007 PET/CT Detects Micrometastases in a Patient with
582 Biochemically Recurrent Prostate Cancer. *Clinical Genitourinary Cancer* **2017**, *15*, e497-e499.

(28) Giesel, FL.; Will, L.; Lawal, I.; Lengana, T.; Kratochwil, C.; Vorster, M.; Neels, O.; Reyneke, F.; Haberkon, U.; Kopka, K.; Sathekge, M. Intraindividual Comparison of ^{18}F-PSMA-1007 and ^{18}F-DCFPyL PET/CT in the Prospective Evaluation of Patients with Newly Diagnosed Prostate Carcinoma: A Pilot Study. *J. Nucl. Med.* **2018**, *59*, 1076-1080.

(29) Kesch, C.; Vinsensia, M.; Radtke, JP.; Schlemmer, HP.; Heller, M.; Ellert, E.; Holland-Letz, T.; Duensing, S.; Grabe, N.; Afshar-Oromieh, A.; Wieczorek, K.; Schäfer, M.; Neels, OC.; Cardinale, J.; Kratochwil, C.; Hohenfellner, M.; Kopka, K.; Haberkorn, U.; Hadaschik, BA.; Giesel, FL. Intraindividual Comparison of ^{18}F-PSMA-1007 PET/CT, Multiparametric MRI, and Radical Prostatectomy Specimens in Patients with Primary Prostate Cancer: A Retrospective, Proof-of-Concept Study. *J. Nucl. Med.* **2017**, *58*, 1805-1810.

(30) Giesel, FL.; Knorr, K.; Spohn, F.; Will, L.; Maurer, T.; Flechsig, P.; Neels, O.; Schiller, K.; Amaral, H.; Weber, WA.; Haberkorn, U.; Schwaiger, M.; Kratochwil, C.; Choyke, P.; Kramer, V.; Kopka, K.; Eiber, M. Detection Efficacy of ^{18}F-PSMA-1007 PET/CT in 251 Patients with Biochemical Recurrence of Prostate Cancer After Radical Prostatectomy. *J. Nucl. Med.* **2019**, *60*, 362-368.

(31) Freitag, MT.; Kesch, C.; Cardinale, J.; Flechsig, P.; Floca, R.; Eiber, M.; Bonekamp, D.; Radtke, JP.; Kratochwil, C.; Kopka, K.; Hohenfellner, M.; Stenzinger, A.; Schlemmer, HP.; Haberkorn, U.; Giesel, F. Simultaneous Whole-Body ^{18}F-PSMA-1007-PET/MRI with Integrated High-Resolution Multiparametric Imaging of the Prostatic Fossa for Comprehensive Oncological Staging of Patients with Prostate Cancer: A Pilot Study. *Eur. J. Nucl. Med. Mol. Imaging* **2018**, *45*, 340-347.

(32) Giesel, FL.; Will, L.; Paddubny, K.; Kremer, C.; Rathke, H.; Radtke, JP.; Kopka, K.; Haufe, S.; Haberkorn, U.; Kratochwil, C. [18F]PSMA-1007 PET Improves the Diagnosis of Local Recurrence and Lymph Node Metastases in a Prostate Cancer Patient With a History of Bilateral Hip Arthroplasty. *Clin. Genitourin Cancer* **2018**, *16*, 111-113.

(33) Olberg D. E.; Arukwe, J. M.; Grace, D.; Hjelstuen, O. K.; Solbakken, M.; Kindberg, G. M.; Cuthbertson, A. One Step Radiosynthesis of 6-[^{18}F]Fluoronicotinic Acid 2,3,5,6-Tetrafluorophenyl Ester ([^{18}F]F-Py-TFP): A New Prosthetic Group for Efficient Labeling of Biomolecules with Fluorine-18. *J. Med. Chem.* **2010**, *53*, 1732-1740.

(34) Barinka, C.; Byun, Y.; Dusich, C. L.; Banerjee, S. R.; Chen, Y.; Castanares, M.; Kozikowski, A. P.; Mease, R. C.; Pomper, M. G.; Lubkowski, J. Interactions Between Human Glutamate Carboxypeptidase II and Urea-Based Inhibitors: Structural Characterization. *J. Med. Chem.* **2008**, *51*, 7737-7743.

(35) Pavlicek, J.; Ptacek, J.; Cerny, J.; Byun, Y.; Skultetyova, L.; Pomper, M. G.; Lubkowski, J.; Barinka, C. Structural Characterization of P1'-Diversified Urea-Based Inhibitors of Glutamate Carboxypeptidase II. *Bioorganic & Medicinal Chemistry Letters* **2014**, *24*, 2340-2345.

(36) Plechanovová, A.; Byun, Y.; Alquicer, G.; Škultétyová, L.; Mlčochová, P.; Němcová, A.; Kim, H.-J.; Navrátil, M.; Mease, R.; Lubkowski, J.; Pomper, M.; Kovalinka, J.; Rulišek, L.; Bařinka, C. Novel Substrate-Based Inhibitors of Human Glutamate Carboxypeptidase II with Enhanced Lipophilicity. *J. Med. Chem.* **2011**, *54*, 7535-7546, doi:10.1021/jm200807m (2011).

(37) Zhang, A. X.; Murelli, R. P.; Barinka, C.; Michel, J.; Cocleaza, A.; Jorgenson, W. L.; Lubkowski, J.; Spiegel, D. A. A Remote Arene-Binding Site on Prostate Specific Membrane

Antigen Revealed by Antibody-Recruiting Small Molecules. *J. Am. Chem. Soc.* **2010**, *132*, 12711-12716.

(38) Novakova, Z.; Cerny, J.; Choy, C. J.; Nedrow, J. R.; Choi, J. K.; Lubkowski, J.; Berkaman, C. E. Design of Composite Inhibitors Targeting Glutamate Carboxypeptidase II: The Importance of Effector Functionalities. *The Febs Journal* **2015**, *283*, 130-143.

(39) Ganguly, T.; Dannoon, S.; Hopkins, M. R.; Murphy, S.; Cahaya, H.; Blecha, J. E.; Jivan, S.; Drake, C. R., Barinka, C.; Jones, E. F.; VanBrocklin, H. F.; Berkman, C. E. A High-Affinity [^{18} F]-Labeled Phosphoramidate Peptidomimetic PSMA-Targeted Inhibitor for PET Imaging of Prostate Cancer. *Nucl. Med. Biol.* **2015**, 42, 780-787.

(40) Navrátil, M.; Ptáček, P.; Šácha, P.; Starková, J.; Lubkowski, J.; Bařinka, C.; Konvalinka, J. Structural and Biochemical Characterization of the Folyl-Poly-Gamma-L-Glutamate Hydrolyzing Activity of Human Glutamate Carboxypeptidase II. *The Febs Journal* **2014**, *281*, 3228-3242.

(41) Barinka, C.; Hlouchova, K.; Rovenska, M.; Majer, P.; Daunter, M.; Hin, N.; Ko, Y.-S.; Tsukamoto, T.; Slusher, B. S.; Konvalinka, J.; Lubkowski, J. Structural Basis of Interactions Between Human Glutamate Carboxypeptidase II and its Substrate Analogs. *J. Mol. Biol.* **2008**, *376*, 1438-1450.

(42) Rahbar, K.; Afshar-Oromieh, A.; Seifert, R.; Wagner, S.; Schäfers, M.; Bögemann, M.; Weckesser, M. Diagnostic Performance of 18F-PSMA-1007 PET/CT in Patients with Biochemical Recurrent Prostate Cancer. *Eur. J. Nucl. Med. Mol. Imaging* **2018**, *45*, 2055-2061.

(43) Rahbar, K.; Afshar-Oromieh, A.; Bögemann, M.; Wagner, S.; Schäfers, M.; Stegger, L.; Weckesser, M. ^{18}F-PSMA-1007 PET/CT at 60 and 120 Minutes in Patients with Prostate Cancer:

Biodistribution, Tumour Detection and Activity Kinetics. *Eur. J. Nucl. Med. Mol. Imaging* **2018**, *45*, 1329-1334.

(44) Cardinale, J.; Schäfer, M.; Kopka, K.; Eder, M.; Bauder-Wüst, U.; Eisenhut, M.; Benesova, M.; Haberkorn, U.; Fiesel, F. 18F-Tagged Inhibitors of Prostate Specific Membrane Antigen (PSMA) and their Use as Imaging Agents for Prostate Cancer. WO2017/054907 A1.

(45) Eder, M.; Schäfer, M.; Bauder-Wüst, U.; Hull, W.-E.; Wängler, C.; Mier, W.; Haberkorn, U.; Eisenhut, M. ^{68}Ga-Complex Lipophilicity and the Targeting Property of a Urea-Based PSMA Inhibitor for PET Imaging. *Bioconjugate Chem.* **2012**, *23*, 688-697.

(46) Tykvart, J.; Šácha, P.; Bařinka, C.; Knedlík, T.; Starková, J.; Lubkowski, J.; Konvalinka, J. Efficient and Versatile One-Step Affinity Purification of *in Vivo* Biotinylated Proteins: Expression, Characterization and Structure Analysis of Recombinant Human Glutamate Carboxypeptidase II. *Protein Expression and Purification* **2012**, *82*, 106-115.

(47) Krug, M.; Weiss, M. S.; Heinemann, U; Mueller, U. XDSAPP: A Graphical User Interface for the Convenient Processing of Diffraction Data Using XDS. *J. Appl. Crystallogr.* **2012**, *45*, 568-572.

(48) Emsley, P.; Lohkamp, B.; Scott, W. G; Cowtan, K. Features and Development of Coot. *Acta Crystallographica. Section D, Biological Crystallography* **2010**, *66*, 486-501.

(49) Murshudov, G. N.; Skubák, P.; Lebedev, A. A.; Pannu, N. S.; Steiner, R. A.; Nicholls, R. A.; Winn, M. D.; Long, F.; Vagin, A. A. REFMAC5 for the Refinement of Macromolecular Crystal Structures. *Acta Crystallographica. Section D, Biological Crystallography* **2011**, *67*, 355-367.

(50) Schuttelkopf, A. W; van Aalten, D. M. PRODRG: A Tool for High-Throughput Crystallography of Protein-Ligand Complexes. *Acta Crystallographica. Section D, Biological Crystallography* **2004**, *60*, 1355-1363.

(51) Chen, V. B.; Arendall III, W. B.; Headd, J. J.; Keedy, D. A.; Immormino, R. M.; Kapral, G. J., Murray, L. W.; Richardson, J. S.; Richardson, D. C. MolProbity: All-Atom Structure Validation for Macromolecular Crystallography. *Acta Crystallographica. Section D, Biological Crystallography* **2010**, *66*, 12-21.

(52) Schäfer, M.; Bauder-Wüst, U.; Leotta, K.; Zoller, F.; Mier, W.; Haberkorn, U.; Eisenhut, M.; Eder, M. A Dimerized Urea-Based Inhibitor of the Prostate-Specific Membrane Antigen for ^{68}Ga-PET Imaging of Prostate Cancer. *Ejnmmi Res* **2012**, *2*, 23.

Graphical Abstract

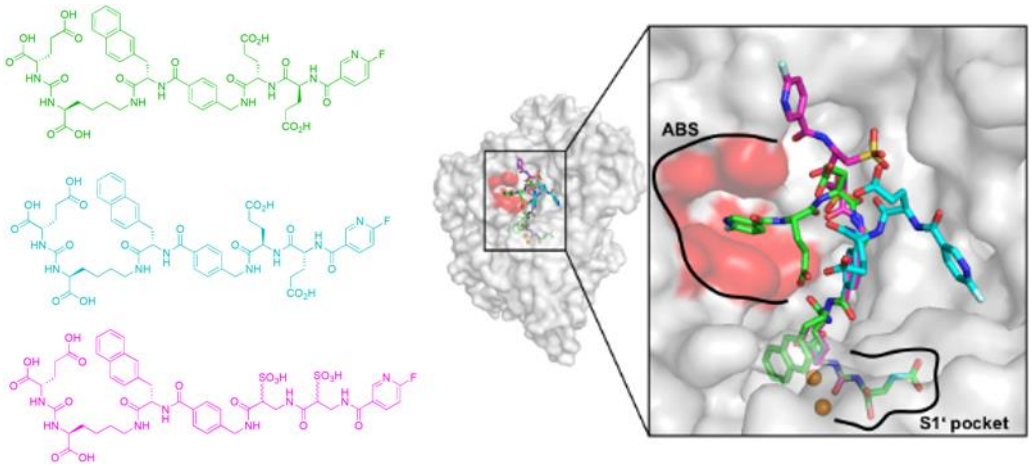

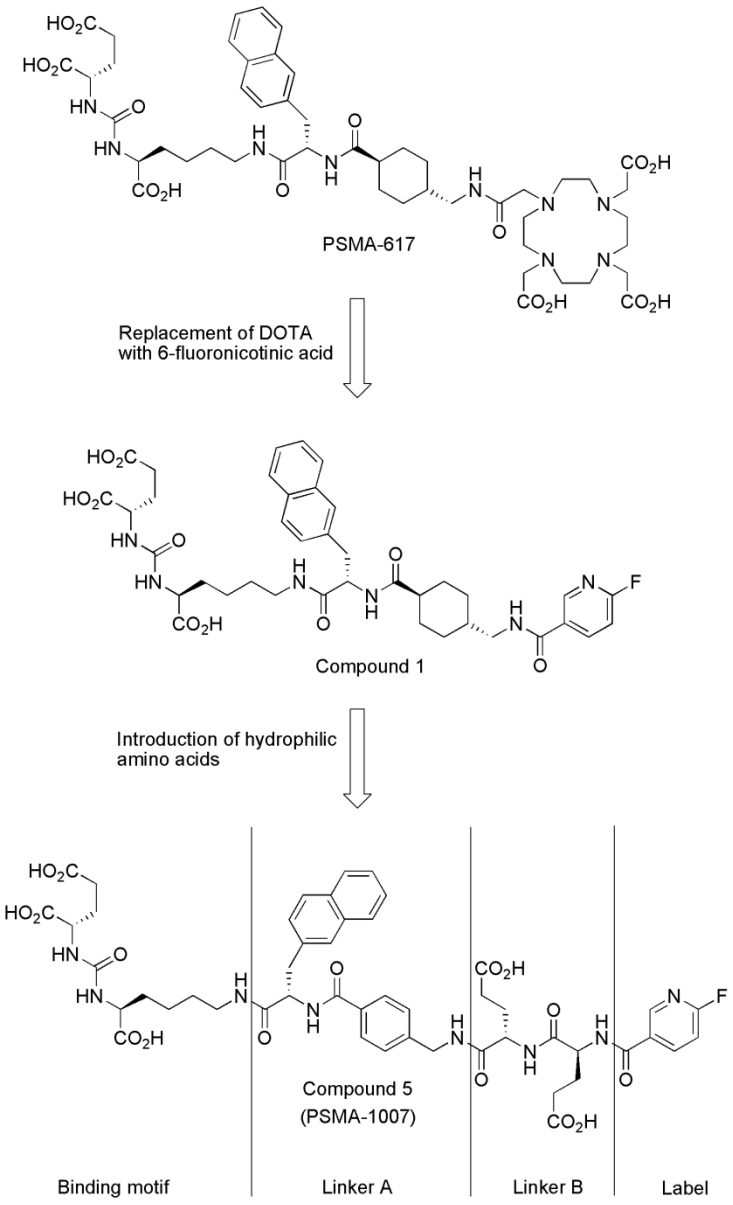

Scheme 1. Key steps in the development of PSMA-1007 and linker structure [23,24]

133x219mm (300 x 300 DPI)

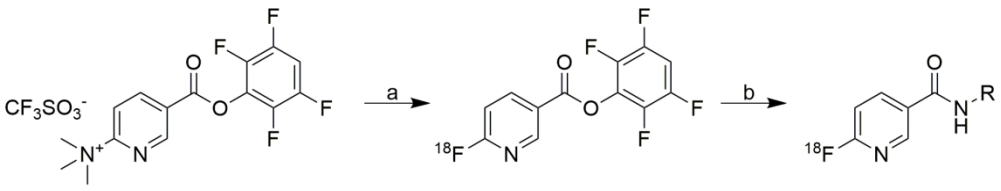

Scheme 2. Labeling Procedure using [^{18}F]F-Py-TFPa

165x30mm (300 x 300 DPI)

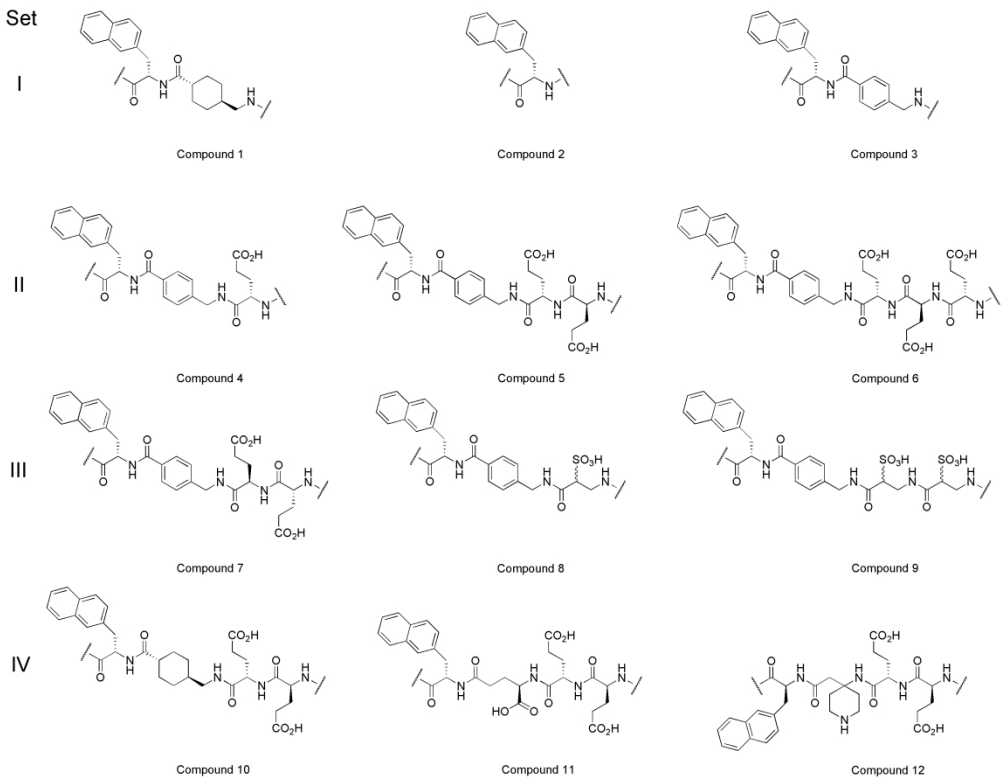

Figure 1. Linker structures (A and B) of the compounds of the present study. Binding motif and label have been omitted for clarity.

300x232mm (300 x 300 DPI)

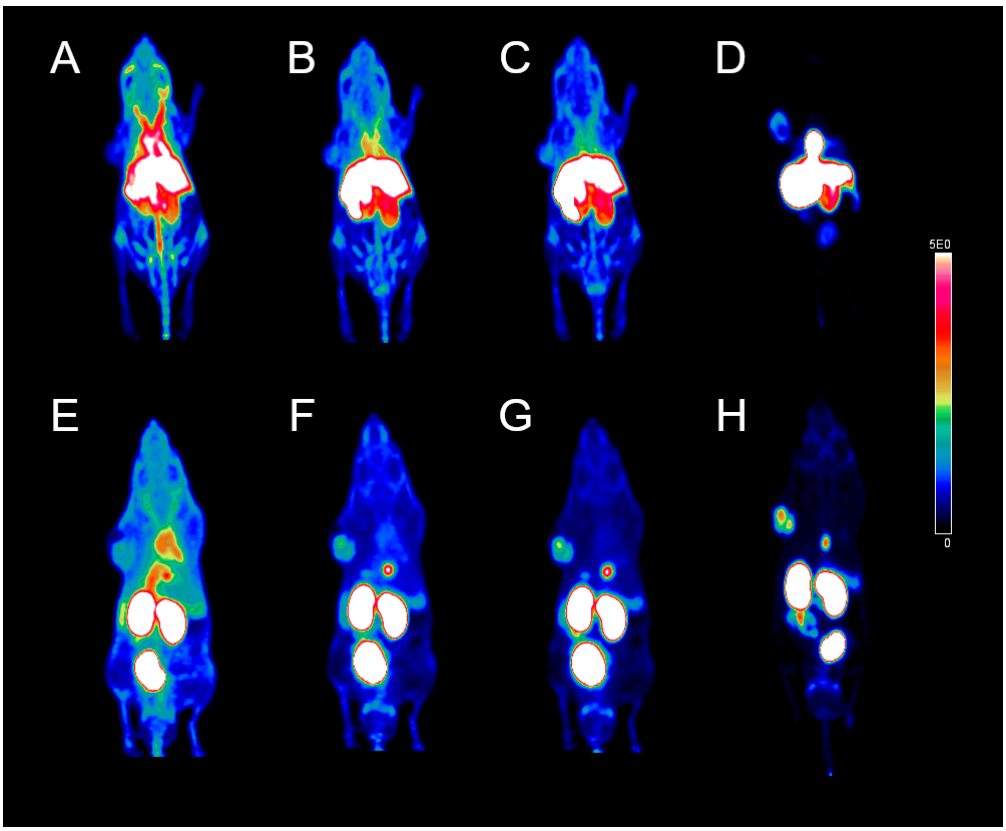

Figure 2. Maximum intensity projections of LNCaP tumor-bearing mice injected with approx. 25 MBq (60 pmol in 100 µl) **[^{18}F]3** (A-D) or **[^{18}F]5** (E-F). Images were acquired 0-20 min (A,E), 20-40 min (B,F), 40-60 min (C,G) and 100-120 min (D,H) p.i.. Images E-H were published previously.[13]

84x69mm (300 x 300 DPI)

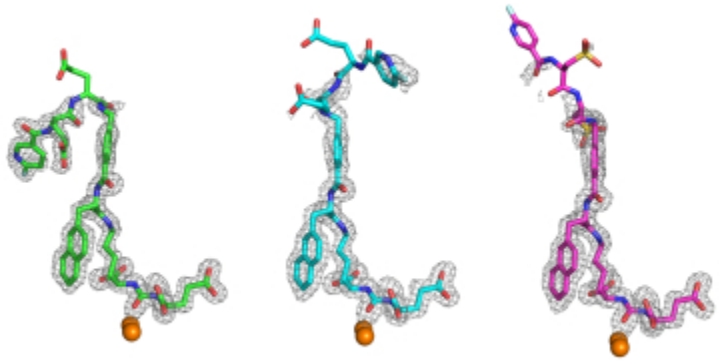

Figure 3. The Fo-Fc omit map (grey) is contoured at 3.0 σ and inhibitors are shown in stick representation with atoms colored red (oxygen), blue (nitrogen), pale cyan (fluorine), and yellow (sulfur). Carbon atoms are colored green, cyan and purple for compound **5** (PDB:ID 5O5T), compound **7** (PDB:ID 5O5R), and compound **9** (PDB:ID 5O5U), respectively. The active-site zinc ions are shown as orange spheres. Notice the absent electron density for some distal inhibitor parts implying its positional flexibility due to missing interactions with the enzyme.

31x18mm (300 x 300 DPI)

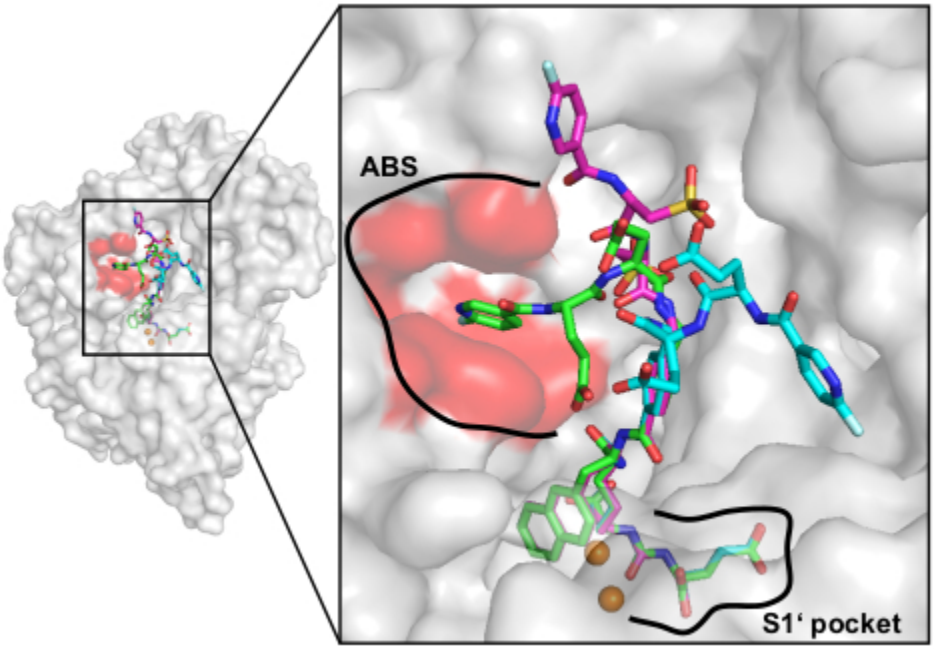

Figure 4. The superposition of PSMA/inhibitor complexes (from PDB-IDs 5O5T, 5O5R and 5O5U). PSMA molecules in individual complexes were superpositioned on corresponding C-α atoms. PSMA is shown in semitransparent surface representation and individual inhibitors in stick representation with carbon atoms colored green, cyan and purple for **5**, **7**, and **9**, respectively. The arene binding site (ABS) is marked red. Notice different positioning of the distal part of the inhibitors, while the PSMA binding motifs up to the phenyl ring fully overlap.

41x30mm (300 x 300 DPI)

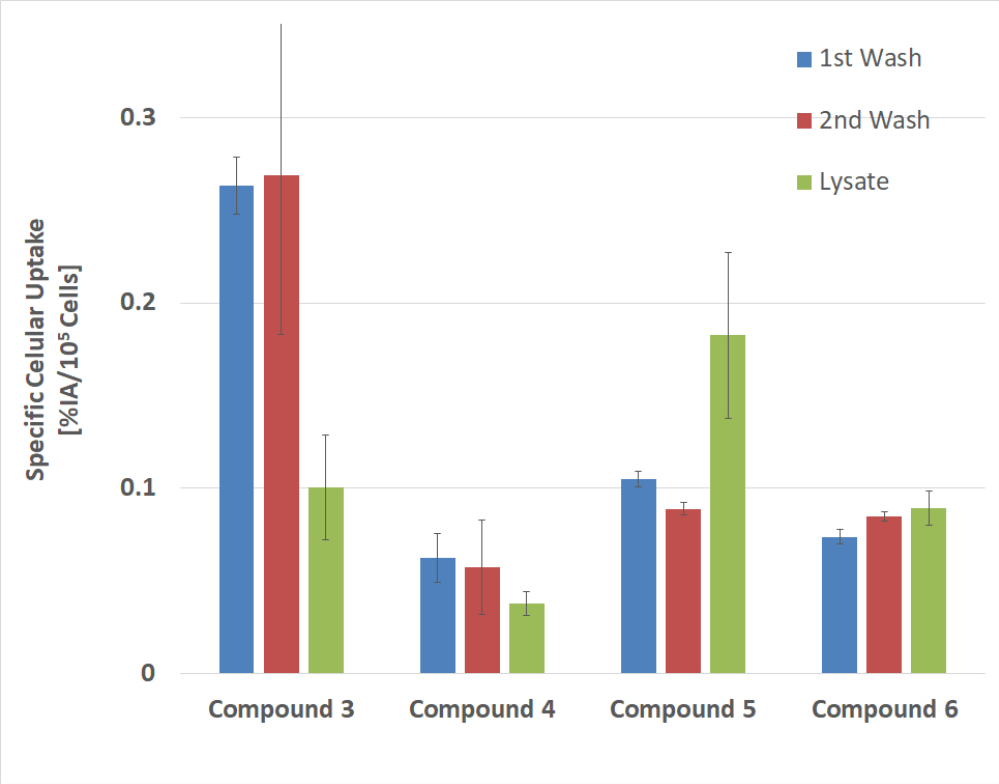

Figure 5. Example of a cell binding assay (n = 1); All compounds were measures as triplet. 1st and second wash corresponds to surface bound activity, lysate to internalized activity.

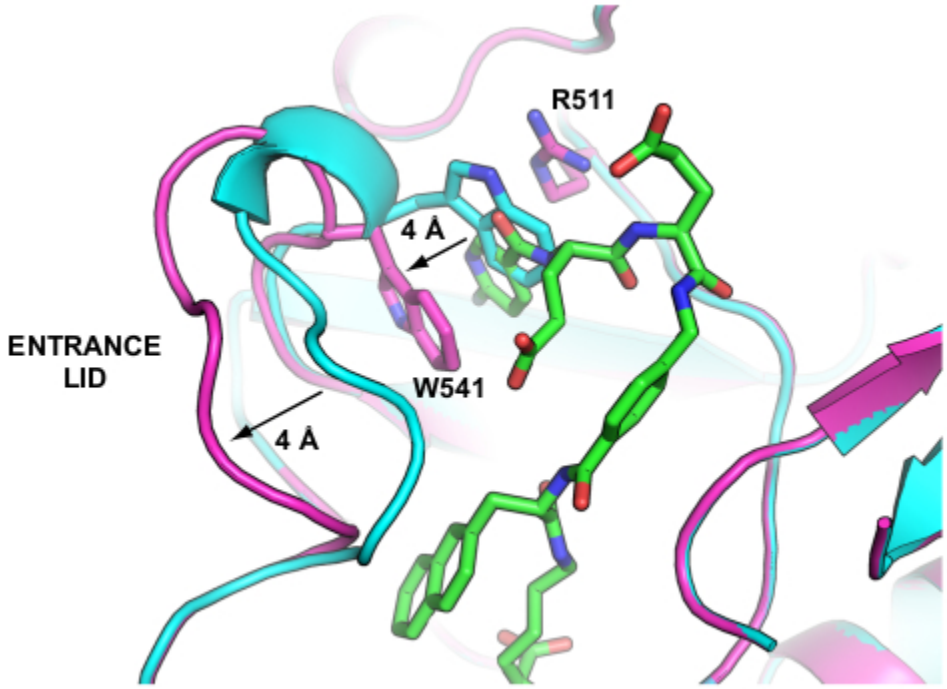

Figure 6. Positional flexibility of the entrance lid (amino acids W541-G548) is critical for the formation of the arene-binding site upon inhibitor binding. Superposition of PSMA complexes with compound **5** (PSMA purple, compound **5** green, PDB-ID: 5O5U) and compound **7** (PSMA cyan; compound **7** inhibitor omitted for clarity, only PSMA part of complex visualized, PDB-ID 5O5R). The protein is shown in cartoon representation and compound **5** in stick representation. Notice 4 Å movement of the entrance lid upon compound **5** binding leading to the formation of the arene-binding site.

41x30mm (300 x 300 DPI)

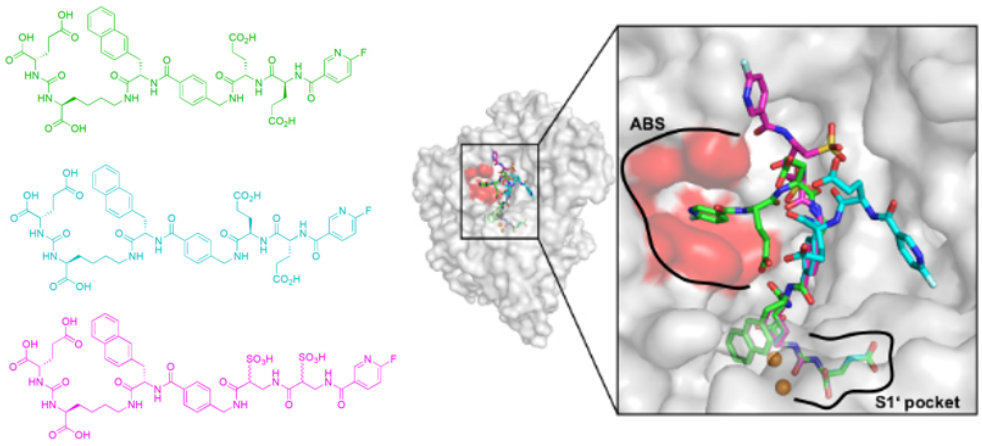

Grapgical Abstract

138x60mm (150 x 150 DPI)